Experimental Detection and Control of Trions and Fermi-Edge Singularity in Single-Barrier GaAs/AlAs/GaAs Heterostructures Using Photocapacitance Spectroscopy

Amit Bhunia,[1] Mohit Kumar Singh,[1] Y. Galvão Gobato,[2,5] Mohamed Henini,[3,4] and Shouvik Datta[1,*]

[1]*Department of Physics & Center for Energy Science, Indian Institute of Science Education and Research, Pune 411008, Maharashtra, India*

[2]*Departamento de Física, Universidade Federal de São Carlos, 13560-905 São Carlos, SP, Brazil*

[3]*School of Physics and Astronomy, University of Nottingham, Nottingham NG7 2RD, UK*

[4]*UNESCO-UNISA Africa Chair in Nanosciences & Nanotechnology Laboratories, College of Graduate Studies, University of South Africa (UNISA), Muckleneuk Ridge, PO Box 392, Pretoria, South Africa*

[5]*High Field Magnet Laboratory (HFML-EMFL), Radboud University, 6525 ED Nijmegen, The Netherlands*

(Received 9 March 2018; revised manuscript received 9 July 2018; published 17 October 2018; corrected 31 October 2018)

We show how photocapacitance spectra can probe and manipulate two dimensional excitonic complexes and Fermi-edge singularities as a function of applied bias even at a temperature of 100 K. For lower density regimes ($<1 \times 10^{11}$ cm^{-2}), the appearance of two distinct peaks in the spectra are identified as a signature of coexistence of both excitons and positively charged trions. We find the binding energy of these trions to be approximately 2.0 meV, which matches well with known estimates. For higher density regimes ($>1 \times 10^{11}$ cm^{-2}), we observe a sharp spectral transition from trions to asymmetrically shaped Fermi-edge singularities in photocapacitance spectra above a particular reverse bias. However, these signatures of indirect excitonic states are absent from photoluminescence spectra. Such dissimilarities clearly point out that different many-body physics govern these two spectral measurements. We also argue why such quantum-confined dipoles of spatially indirect trions can have thermodynamically finite probability to survive even around 100 K. Finally, our observations demonstrate that photocapacitance spectroscopy, which was rarely used to detect trions in the past, can also be useful to detect the traces of these spatially indirect excitonic complexes as well as Fermi-edge singularities. This is mainly due to the enhanced sensitivity of these capacitive measurements to "dipolar" changes of excitonic complexes in these heterojunctions. Thus, our studies clearly open up future possibilities for electro-optical modulation and detection of trions and Fermi-edge singularities in several other heterostructures for next-generation optoelectronic applications.

DOI: 10.1103/PhysRevApplied.10.044043

I. INTRODUCTION

Experimental study of neutral excitons (say X^0) and charged excitons such as positively or negatively charged trions (X^+ or X^-) inside two-dimensional (2D) semiconductor quantum structures are becoming important for understanding many-body physics of excitonic complexes [1,2] as well as for applications of excitonic devices [3]. The existence of trions was first demonstrated in semiconductors by Lampert [4]. Since then, there have been numerous reports on the optical spectroscopic signatures of trions at low temperatures of a few kelvins. This is mainly because of small binding energies (approximately 1–2 meV) of trions in III-V material systems [5–7]. However, trions in 2D monolayers of transition metal dichalcogenides (TMDC) can have much larger binding energies [8,9] of approximately 20–50 meV. Such large binding energies of excitons and trions in TMDC materials can make it much easier not only to study the many-body physics of excitonic complexes even at room temperature, but also their use in optoelectronic devices. However, there are also reports of some disparities between theoretical and experimental observations of precise signatures of positively or negatively charged trions and their expected binding energies [7]. According to theoretical predictions [10], the binding energy of positively charged trions should be higher due to the larger hole effective mass, but experiments have reported very similar values of binding energies [11] for both X^+ and X^-. At this point, we understand that identifying a trion as X^+ or X^- depends mostly on how electrons and holes are being injected with applied bias based on the device configuration. The presence of these excitonic complexes usually occurs in moderate density regimes, whereas many-body interactions of charge

*shouvik@iiserpune.ac.in

carriers with Fermi sea lead to a Fermi-edge singularity (FES) in high density regimes. This was first predicted by Mahan [12] in degenerate semiconductors. Theory [13,14] and experiments [15–17] of such crossover to FES in III-V semiconductors have mostly been studied at low temperatures of a few kelvin by optical absorption and photoluminescence (PL) spectroscopies.

In the present study, we report that simple photocapacitance spectroscopy can be used to detect the specific signature of positively charged trions of indirect excitons (IX^+) at moderate levels of carrier densities ($<1\times10^{11}$ cm^{-2}) as well as FESs in higher levels of carrier densities ($>1\times10^{11}$ cm^{-2}) in a single-barrier GaAs/AlAs *p-i-n* heterostructure. We had already demonstrated [18] that photocapacitance spectroscopy can be used as a sensitive electro-optical tool to probe spatially indirect excitons formed across the AlAs potential barrier in a GaAs/AlAs/GaAs heterostructure even at room temperature. The work described in this manuscript is a direct continuation of that recent work [18]. Here, we argue why photocapacitance can sense these IX^+s even at 100 K, which are not possible to detect with PL. Formations of triangular quantum wells (TQWs) around a Γ-AlAs potential barrier also help these spatially indirect trions to survive, even at such a temperature. We establish that photocapacitance spectroscopy is a more sensitive experimental technique for detecting trions and many-body effects such as FES than PL in such heterostructures. We also demonstrate that it is possible to probe and monitor the dielectric properties of strongly correlated, interacting dipoles of excitons, trions, and FESs using such capacitance-based techniques even at 100 K. In fact, these dipolar properties of excitonic complexes are mostly neglected in standard optical emission-based spectroscopic techniques used in past studies to probe excitonic Bose-Einstein condensation (BEC), excitonic lasing, etc.

II. SAMPLE AND EXPERIMENTAL METHODS

The heterostructure we use in this work is grown by molecular beam epitaxy on a semi-insulating GaAs (311)A substrate. A highly doped 1.5-μm-buffer layer of *p*-GaAs (4×10^{18} cm^{-3}) is first grown on the substrate. This layer is used as the bottom electrical contact for our measurements. This is followed by a 100-nm-thick *p*-GaAs (1×10^{17} cm^{-3}) layer. Then an 8-nm-thick undoped AlAs potential barrier having 100-nm-thick undoped GaAs spacer layers on both sides are grown. Finally, a 100-nm *n*-GaAs (2×10^{16} cm^{-3}) layer and a 0.5-μm highly n-doped GaAs (4×10^{18} cm^{-3})

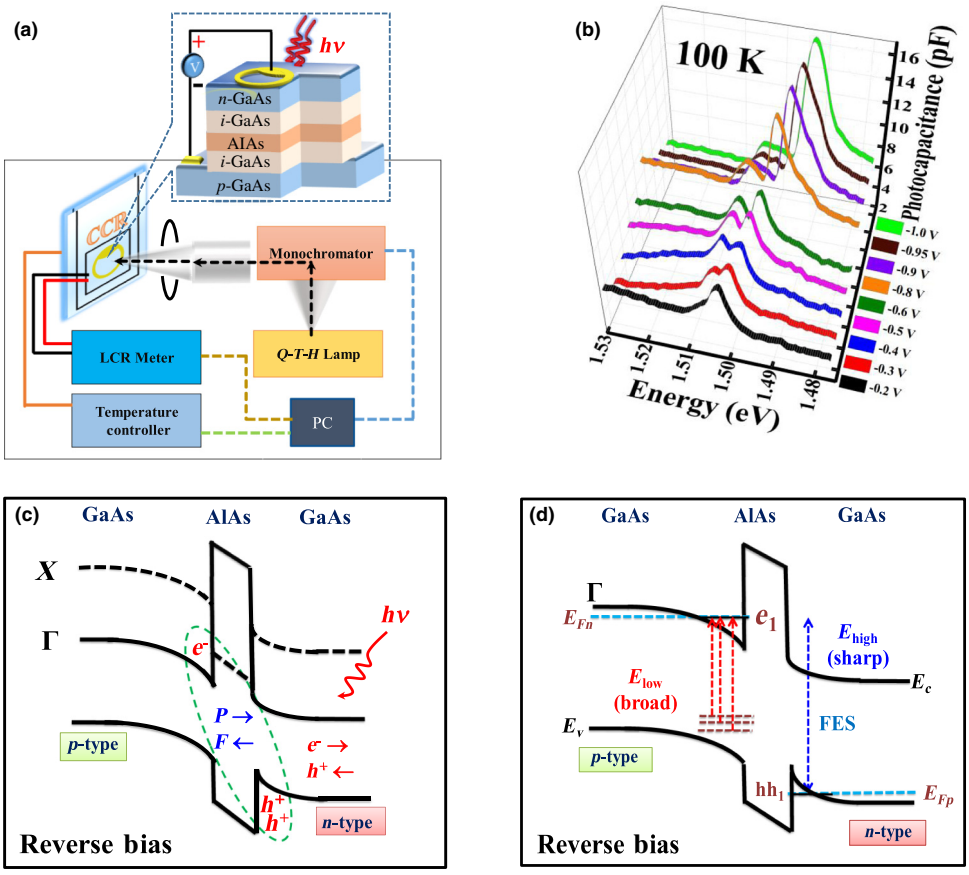

FIG. 1. (a) A schematic diagram of the experimental setup for photocapacitance measurements is given here. Inset shows the sample structure. (b) Variation of excitonic photocapacitance spectra with optical excitation energy for different reverse biases at 100 K. A single excitonic peak splits into two distinct peaks of exciton and trion with increasing applied biases. A low-energy trion peak evolves into FES-like asymmetric spectra at higher biases. The last four spectra from −0.8 to −1.0 V are vertically shifted by 2 pF for better visibility. (c) Schematic band diagram of the reverse-biased sample under light illumination from the top *n*-GaAs side. This is used to explain the formation of positively charged trions. (d) The origin of the low- and high-energy tails of the FES spectra is schematically explained using a similar diagram. Relevant transitions contributing to low- and high-energy optical absorption tails are depicted with red and blue arrows, respectively.

capping layer are grown to complete this heterostructure. Arrays of circular ring-shaped gold mesas with a diameter of 400 μm and an area of approximately 5×10^{-4} cm^2 are fabricated as top metal contacts. These mesas also facilitate optical access from the top of the device.

We use Agilent's E4980A *LCR* meter with 30 mV of rms voltage at 200-Hz frequency (unless mentioned otherwise) for photocapacitance measurements. Photocapacitance ($C_{\text{photo}} = dQ/dV$) is measured under applied reverse bias while our sample is illuminated from the top *n*-GaAs side. Photocurrent measurements are performed using the same *LCR* meter in the dc mode as well as with a Keithley 2611 source meter. An Acton Research SP2555 monochromator having a 0.5-m focal length (with $\Delta\lambda \sim 1.5$ nm) along with a 1000-W quartz-tungsten-halogen lamp is used for photocapacitance spectroscopy. The spectral response of the lamp-monochromator combination is reasonably smooth and changes slowly and monotonically within the wavelength ranges we use in our experiments. PL spectra are measured using a 35-mW He-Ne gas laser and CCS200 compact spectrometer from Thorlabs with a spectral accuracy <2 nm at 633 nm. For temperature variation, we use a closed-cycle helium gas CS-204S-DMX-20 cryostat from Advance Research Systems along with a Lakeshore (Model-340) temperature controller. A schematic diagram of the GaAs/AlAs single barrier *p-i-n* heterostructure and the experimental set up of photocapacitance measurement are shown in Fig. 1(a).

Photocapacitance spectra at 100 K are measured under an optical intensity of 17.4 μW/cm^2 at a peak wavelength of 830 nm under reverse bias. In this work, we will only focus on the sharp resonant peaklike spectral features in photocapacitance under nonzero biases. We carefully select top mesa contacts for which dc photocurrents are restricted within nanoampere ranges under reasonably small applied biases of a few volts. This prevents unwarranted dielectric screening of Coulomb attractions required to form these excitonic complexes. The applied electric fields corresponding to each bias are estimated by dividing the bias magnitude by the thickness (approximately 208 nm) of the intrinsic region of the heterostructure.

Previously, indirect excitons have usually been created and probed using external gate voltages to tear apart direct excitons formed inside a single quantum well or in coupled quantum wells. However, these procedures often broaden the excitonic spectra and thereby compromise the nature of these excitons. On the other hand, here the applied electric fields are mainly utilized to push electrons and holes toward each other to form spatially separated, indirect excitons, trions, and FESs across the Γ-AlAs potential barrier. We have already shown [18] that this actually results in uncharacteristic sharpening of the photocapacitance spectral features of indirect excitons with increasing bias. For more detailed comparisons, readers can see Ref. [18].

III. RESULTS AND DISCUSSIONS

A. Bias-dependent splitting in photocapacitance spectra leads to positively charged trions and Fermi-edge singularity at 100 K

Here, we investigate bias-induced formation dynamics of spatially indirect excitons and trions near the GaAs/AlAs/GaAs heterojunction under light and also under applied reverse biases around 100 K. In Fig. 1(b), changes in photocapacitance spectra under different applied reverse biases are shown. As the magnitude of the reverse bias increases from −0.1 V to higher values, a single resonant peaklike excitonic spectrum is split up into two distinctly separate peaks. This kind of peak splitting with increasing bias is clearly absent at room temperature [18]. Initially, the spectral shapes of these peaks remain nearly symmetric until the bias value of −0.6 V. After this, an asymmetric spectral shape emerges where the low-energy spectral tails rise slowly and the high-energy side falls sharply. In addition, an enhancement of the low-energy peak is clearly noticeable around −0.8 V and beyond. On the other hand, the higher-energy peak gradually almost vanishes at larger biases.

To understand the above observations, a schematic band diagram of the GaAs/AlAs/GaAs heterojunction is drawn in Fig. 1(c) following previous reports [18–20]. We will not go into details of these *X*- and Γ-valley contributions on the carrier transport, which has already been well investigated and discussed [18]. Under the above-mentioned experimental conditions, we expect [18] the formation of hole accumulation layers in the form of 2D hole gas (2DHG) within the GaAs TQW near the Γ-AlAs barrier in the top *n*-type GaAs layer above a certain bias. Similarly, we expect to have an electron accumulation layer as a 2D electron gas (2DEG) forming inside the TQW on the *p*-type GaAs side. These accumulated electrons and holes can form hydrogenic bound states of indirect excitons (IX^0) due to their mutual Coulomb attractions as reported earlier [18]. This schematic diagram matches with the standard solution of self-consistent one-dimensional Schrodinger and Poisson equations as described in earlier reports [21,22]. The 2DEG is spatially separated by an 8-nm-thin AlAs barrier from the 2DHG. The presence of this extra potential barrier in the tunnel diode structure may introduce further complexities in such calculations. Additional charge accumulations in TQWs can lead to solutions of the Poisson equation that are not [21] fully self-consistent with the Schrodinger equation for such resonant tunneling structures. Due to the dominant presence of the Γ-AlAs potential barrier [18], the equilibrium charge transfer and band alignment of this heterojunction are significantly different from that of a normal *p-i-n* diode. We also expect the presence of both electrons and holes within respective TQWs inside this heterojunction. Therefore, we purposely avoid any quantitative estimation of

carrier density using a standard capacitance-voltage plot, which is strictly based on a depletion approximation and the presence of a single type of majority carrier.

However, we understand that large numbers of electrons and holes can accumulate in these TQWs to form 2DEG and 2DHG, respectively, with increasing reverse biases. As a result, corresponding carrier densities in each TQW also increase. So, the charge density of photogenerated carriers per unit area ($\sigma_{\rm ph}$) around the heterojunction for each bias value can be estimated from Fig. 1(b) using the following relationship [8]:

$$\sigma_{\rm ph} e = CV, \tag{1}$$

where e is the electric charge and C is the peak value of excitonic photocapacitance per unit area at each applied bias (V). Following the description in Fig. 1(c), it is important to note here that one can also relate this $\sigma_{\rm ph}$ to the density of dipolar charges per unit area in a standard parallel plate capacitor configuration as

$$\sigma_{\rm ph} = \vec{P} \cdot \hat{z}, \tag{2}$$

where $\vec{P}$ is the effective polarization of these excitonic dipoles around the AlAs barrier and $\hat{z}$ is the unit vector along the growth direction.

At a high enough injected carrier density, another peak at the low-energy side starts to appear. This happens with $\sigma_{\rm ph} > 3 \times 10^{10}$ cm^{-2} or reverse biases greater than $|-0.3|$ V as shown in Fig. 1(b). Evidently, concentrations of holes in the 2DHG become larger compared to those of electrons in 2DEG. This is because the sample is optically excited from the top n-GaAs side only and bias is also applied in the reverse direction. Such excess of one type of carrier (in our case holes) favors the formation of positively charged trions, which can be controlled by both light or bias [23]. As a result of this excess hole density in 2DHG, we now relate the sharp resonant spectral features on the low energy side of the spectra with positively charged indirect excitons or trions (IX^+). Until the bias value reaches -0.6 V or $\sigma_{\rm ph} \sim 8 \times 10^{10}$ cm^{-2}, both peaks look nearly symmetric, even though we see that the trion peak is getting bigger than the exciton peak. This low energy IX^+ state is more energetically favorable and tends to dominate at even higher applied biases.

Subsequently, after the reverse bias around -0.8 V, we observe another drastic change in the spectral behavior as is evident in Fig. 1(b). The low energy trion peak rises significantly, whereas the exciton peak almost vanishes around $\sigma_{\rm ph} \sim 1.2 \times 10^{11}$ cm^{-2}. Moreover, the spectral shape of this trion peak gradually becomes asymmetric in nature. This type of spectral transition is usually [15–17,24] identified with Fermi-edge singularities at high enough carrier densities. Correspondingly, in our photocapacitance spectra, we see similar sharp, asymmetric enhancement of the trion peak once the photogenerated density approaches $\sigma_{\rm ph} \sim 1 \times 10^{11}$ cm^{-2}. In the present case, it is likely that at high photogenerated carrier densities, localized hole states of 2DHG or holes in shallow impurity states can experience enhanced Coulomb attraction with the Fermi sea of electrons in 2DEG at such low temperatures. As a result, we observe a significant enhancement of optical absorption of this trion-related FES. Previously, Yusa *et al.* [15] reported an asymmetric line shape in the absorption spectra that showed a fast rise in the low-energy side and a slow fall in the high-energy side. Chen *et al.* [16] and Skolnick *et al.* [17] observed a slow rise in the low-energy side and a fast fall in the high-energy side of the PL spectra. Usually, in the high-density limit, enhanced carrier-carrier scattering broadens the high-energy tail of FES. However, we notice that photocapacitance spectra in Fig. 1(b) have a much sharper high-energy edge in a system consisting of both 2DEG and 2DHG. In addition, we still see the remnant excitonic state above the FES. At the end of this section, we will again discuss how sub-band-gap localized states may significantly modify the photocapacitance spectral broadening in the lower energy side of FES.

Nevertheless, in the common understanding of FES inside a quantum well structure, a sea of electrons in the conduction band is usually attracted to a single localized hole state near the valence band. This usually shows a power law singularity [15] of the form

$$A(\omega) = \frac{1}{|\omega - \omega_0|^{\alpha}}, \tag{3}$$

in the absorption spectra where ω is the angular frequency of incident light, ω_0 is the resonant angular frequency of the absorption peak, and α is a power law exponent. At -0.8 V, we find $\alpha \approx 0.4$, albeit from the low-energy tail of the FES spectra. This value, however, matches with the literature [15]. At this stage, it is important to reiterate that here we are actually dealing with the dual presence of both 2DEG and 2DHG. In a way, we are looking at how a Fermi sea of electrons inside a 2DEG interacts with excess holes localized around 2DHG. We will explain this in more detail at the end of this section.

We also note that the FWHMs (of approximately 8 meV) of these FES peaks are somewhat lower than the corresponding thermal width of $k_B T = 8.7$ meV at 100 K. So, we can assume that this FWHM may provide an estimate of the Fermi energy following the discussion by Skolnick *et al.* [17]. The 2D Fermi energy is usually calculated using the expression (for spin ½ particles)

$$E_F = \frac{\pi \hbar^2 \sigma_{\rm ph}}{m^*}, \tag{4}$$

where $\hbar$ is the reduced Planck's constant and $\sigma_{\rm ph}$ is the dipolar charge density per cm^2. Here, for these excitonic dipoles around the AlAs barrier, we have used

$m^* = \mu$ as the reduced mass of holes and electrons of approximately $0.056m_0$ in GaAs, where m_0 is the free electron mass. Therefore, using Eq. (4), we find that FWHM $\sim E_F = 8$ meV corresponds to $\sigma_{\rm ph} \sim 1.86 \times 10^{11}$ cm^{-2} (following the discussion of Skolnick *et al.* in Ref. [17]). This estimate matches closely with the 1.82×10^{11} cm^{-2} deduced from Eq. (1) at a bias of -1.0 V around where the prominent signatures of FES-like asymmetric spectra are visible.

In TQWs, we understand that only the first few states of these 2DEG or 2DHG can remain strongly quantum confined, i.e., behave as 2D in nature. Higher-energy states in TQWs are less localized as the well width becomes wider [21]. We understand this from the quantized energy E_n and nth eigenfunctions $\psi_n(z)$ of an infinite barrier TQW [22], which are given by

$$E_n \sim \sqrt[3]{\left\{\left(\frac{\hbar^2}{2m^*}\right)\left[\frac{3\pi eF_z}{2}\left(n-\frac{1}{4}\right)\right]^2\right\}}, \tag{5}$$

and

$$\psi_n(z) = \mathrm{Ai}\left(\frac{2m^* eF_z}{\hbar^2}\left(z - \frac{E_n}{eF_z}\right)\right), \tag{6}$$

where $n = 1,2,3\ldots$, Ai(z) are the Airy functions, m^* is the effective mass of the electron or hole, e is the electronic charge, F_z is the electric field along the growth direction along the z axis, and $\hbar$ is the reduced Planck's constant. The ratio of the first excited energy to the ground-state energy is $E_2/E_1 = \sqrt[2/3]{(7/3)} \sim 1.76$. Therefore, it is expected that, in practice, with a finite barrier TQW such as those shown in Fig. 1(c), only the ground-state energy may remain strongly bound and quantum confined. However, with increasing bias and charge accumulations around the AlAs barrier, the quasi-Fermi-levels can penetrate these TQWs at the onset of FES. As a result, we also observe a sharp transition around a reverse bias of -0.8 V where the exciton-trion spectra suddenly convert into asymmetric FES spectra. This is because, with increasing bias, the quasi-Fermi-level E_{Fn} (E_{Fp}) of electrons (holes) can get pinned to the discrete ground-state energy of 2DEG (2DHG) in these TQWs. However, the quasi-Fermi-level separation $(E_{Fn} - E_{Fp})$ can vary along with the ground-state energy levels of these electron and hole TQWs as shown in Fig. 1(d). As a result, we find that $(E_{Fn} - E_{Fp})$ can keep on increasing with the increase of the reverse bias (electric field) as per Eq. (5). In the absence of any quantum confined excited states in these shallow TQWs, the maximum optical absorption energy for indirect excitons can then be limited by

$$E_{\rm Opt}^{\rm Max} = E_g + E_1^e + E_1^{HH} \equiv (E_{Fn} - E_{Fp}), \tag{7}$$

where E_g is the bulk band gap of GaAs and E_1^e (E_1^{HH}) is the ground-state energy of electrons (heavy holes). In fact, we observe FES related enhancement at this $E_{\rm Opt}^{\rm Max}$ edge only. In Fig. 1(d), we pictorially depict both the high- and low-energy portions of this FES transition as $E_{\rm high}$ ($= E_{\rm Opt}^{\rm Max}$) and $E_{\rm low}$ following our schematic diagram given in Fig. 1(c). We assume that quantum confined holes in 2DHG can be further localized to shallow impurity states or interface trap states or to states related to alloy disorder inside 2DHG near the valence band edge. Any optical absorption from such shallow states near the 2DHG to E_1^e can couple the holes left in these localized states with the 2DEG to create the FES. Thus Fig. 1(d) can also explain the broad low-energy tail ($E_{\rm low}$) of the FES spectra as compared to its much sharper high-energy side ($E_{\rm high}$) as found in Fig. 1(b). Such relative sharpness of the high-energy edge of FES can be traced back to the intrinsic sharpness of the respective Fermi edges as given in Eq. (7). All of these understandings are schematically described in Fig. 1(d) and fully support our above explanations based on the formation of positively charged IX^+ at lower bias levels.

B. Redshift and binding energy of indirect trions at 100 K

To picture the above explanations, in Fig. 2(a), we use a 2D color-filled contour plot of Fig. 1(b). This graphic presentation is essential for better visibility of spectral splitting, the redshift of the low energy IX^+ peak, and energy separation of both exciton and trion peaks. Eventually, the low-energy trion peak leads to FES with increasing reverse biases. The dashed lines are drawn to guide the eyes only. A clear redshift of IX^+ spectra with the applied bias is visible as mentioned above, whereas there is hardly any shift in peak energy for the IX^0 line. At this stage, it is not clear why the excitonic peak at slightly higher energy is not at all affected by increasing the electric field. The applied voltage-dependent spectral energy separation between two peaks clearly changes and increases with increasing bias as evidenced from the two dashed lines drawn in Fig. 2(a).

Following Bugajski and Reginski [25], we now discuss the transformation of trions into FES spectra. In the parabolic band approximation, the Fermi energy E_{Fn} of electrons in the bulk can be written in the form of a low energy onset of absorption (ϵ_F) and emission edge (ϵ_g) as

$$E_{Fn} = (\varepsilon_F - \varepsilon_g)\left(1 + \frac{m_e^*}{m_h^*}\right)^{-1}, \tag{8}$$

where (m_e^*/m_h^*) is the effective mass ratio of electrons and holes of GaAs. The Fermi energy varies with the photogenerated carrier density. As discussed above, we are driving both photogenerated electrons and holes toward the

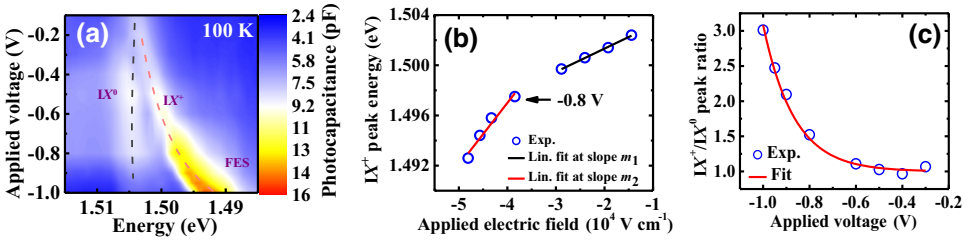

FIG. 2. (a) 2D colored contour plot of Fig. 1(b) is drawn. Two dashed lines are only used for guiding the eyes. Significant redshift of the LX^+ line and the visible splitting of the spectra with bias are clearly pointed out. In higher bias, the symmetric LX^+ line turns into Fermi edge singularity (FES) as the spectral shape become asymmetric. (b) Linear variation of peak energy of positively charged trion with increasing electric field is demonstrated to estimate the permanent dipole moments. There is a clear discontinuity around -0.8 V with a field of -3.8×10^4 V cm^{-1}. This represents a distinct transition from a trionlike peak to a FES-like spectral signature. (c) Bias-activated changes in the ratio of neutral exciton to positively charged trion components of the photocapacitance spectra is shown here.

AlAs barrier. So, the gap between the quasi-Fermi-levels $(E_{Fn} - E_{Fp})$ should increase with increasing bias. However, this change in E_{Fn} can be more compared to changes in E_{Fp}, because, in general, Fermi levels are inversely proportional to the effective mass of the respective carrier and $(m_e^*/m_h^*) \ll 1$. As there is no observed change in the low-energy onset ε_g of photoluminescence (as will be shown later) with increasing reverse bias, we may infer that ε_F may actually blueshift with increasing bias. Here, we assume that any change in the effective mass ratio as a result of bias-induced changes in the shape and size of TQWs is negligible. Consequently, FES-related enhancement of photocapacitance spectra at $E_{\text{Opt}}^{\text{Max}} = (E_{Fn} - E_{Fp})$ should also show a blueshift with increasing reverse bias greater than -0.8 V. However, we see the opposite effect and the high-energy edge of FES actually redshifts. As mentioned above, in this case, FES is a many-body excitonic effect involving both 2DEG and 2DHG. Therefore, understanding the redshift of the FES peak will not be possible without considering how these indirect excitonic complexes and Fermi levels are evolving with increasing bias in such a heterostructure. From our recent report [18] on room temperature indirect excitons, we understand that the electrons and holes of IX^+ can come closer with increasing bias. Consequently, the binding energy of this IX^+ can increase with increasing bias. This can lead to the observed redshift of this trion FES edge due to opening up of an excitonic gap. On the other hand, this significant 10-meV redshift of the IX^+ line with the applied bias in this coupled TQWs structure may also be related to the quantum-confined Stark effect (QCSE) where exciton peaks usually broaden with increasing electric field.

The magnitude of this peak splitting initially increases slowly and then in the higher bias regime it varies significantly as also reported by Yusa *et al.* [15]. With increasing bias, the carrier density also increases, which eventually contributes to strong scattering mechanisms [21]. However, a rigorous explanation of spectral broadening of FES requires understanding the full picture of many-body scattering mechanisms and extrinsic carrier dynamics within such a single barrier heterostructure, which is currently beyond the scope of this study. However, in Fig. 2(b), the spectral redshift of the trion peak energy has been fitted with the linear dipole moment equation

$$E = E_0 + \vec{p} \cdot \vec{F}, \tag{9}$$

where E is the peak energy of IX^+, E_0 is the energy at the zero applied field, $\vec{p}$ is the effective permanent dipole moment of these trions, and $\vec{F}$ is the applied electric field. We can see that $\vec{p}$ and $\vec{F}$ are directed opposite [18] to each other [see Fig. 1(c)]. In addition, $\vec{p}$ is anticipated to be independent of $\vec{F}$ at such a low temperature because of the observed linear variation of E with $\vec{F}$ [see Fig. 2(b)]. Two regions of the bias-dependent photocapacitance spectra have been fitted with two separate straight lines with slopes m_1 and m_2. These slopes actually estimate the values of the respective dipole moments. Slope m_1 corresponds to the dipole moment value of approximately 2.96×10^{-28} C m before the onset of FES. However, we get a substantially larger value of this dipole moment from slope m_2 $\sim 7.97 \times 10^{-28}$ C m for the higher bias region in presence of FES. In the higher electric field regime, there will be more carrier injections to the TQWs. Following Eq. (2) and Fig. 1(d), this eventually contributes to larger dipolar polarizations as compared to that in lower biases.

As can be seen in Fig. 2(c), the peak intensity ratio of the peaks IX^+ and IX^0 varies slowly at the beginning. It then changes significantly upon increasing the applied electric fields. The ratio remains near unity in the low bias side, indicating equal contribution from both excitons and trions. However, with increasing biases, the trions start to dominate the photocapacitance spectra. This is because positive trion formation is always more energetically favorable compared to the excitons. As a result, the peak photocapacitance ratio of trions and excitons is

shown to vary with the applied field, implying the formation of trions at the expense of excitons with the increase of electric field in the reverse bias regime. We try to fit the above variation with a modified Arrhenius rate (R^*) equation following our earlier work [26]

$$R^* \approx \frac{1}{\tau} = \nu^* \exp\left(-\frac{E_a}{k_B}\eta V_{\rm dc}\right), \tag{10}$$

where η is a proportionality factor in units of V^{-1} K^{-1} to ensure correct dimensionality, E_a is the activation energy for transitions activated by bias voltage $V_{\rm dc}$, ν^* is the thermal prefactor representing the heat bath, τ is the time period of the transition, and k_B is the Boltzmann constant. The experimental data on the peak photocapacitance ratio in Fig. 2(c) fits well with such a bias-activated model. The ratio drastically increases around the reverse bias of −0.8 V.

We have already mentioned that exciton peaks gradually decrease and hardly shift in energy with increasing applied bias, whereas the trion peaks are slowly enhanced and redshift drastically after a certain applied bias. This can happen if more and more positively charged trions (IX^+) form at the expense of excitons (IX^0) in the presence of excess holes. Moreover, the trion peak ultimately converts to FES after a certain density regime, which is in our case around 1×10^{11} cm^{-2}. This understanding matches well with explanations provided by Huard *et al.* [27]. Accordingly, we plot the energy difference between two peaks with the estimated Fermi energy for each applied bias in Fig. 3. This is then linearly fitted with the following relation [8,27]:

$$E_{IX^0} - E_{IX^+} = E^b_{IX^+} + E_{Fp}, \tag{11}$$

where $E^b_{IX^+}$ is the positive trion binding energy, E_{IX^0} and E_{IX^+} are peak energies for indirect excitons and positive trions, respectively, and E_{Fp} is the Fermi energy change due to extra holes in the valence band. E_{Fp} is estimated from the photogenerated carrier density using Eqs. (4) and (1) with the effective mass of a hole as $m^*_h \sim 0.45\ m_0$ in GaAs. From the intercept, we estimate the value of an average trion's binding energy of $E^b_{IX^+}$ ∼2.0 meV. However, we are also assuming here that the estimated value of $E^b_{IX^+}$ using the above Eq. (11) is independent of the applied bias. Interestingly, it matches well with an earlier reported value in a GaAs/AlAs system [5–7,11]. This supports our spectroscopic confirmation of the presence of trions (IX^+) using photocapacitance. Whereas previous reports mostly estimate this binding energy from PL measurements, here we show that trion binding energy can also be determined from photocapacitance spectroscopy.

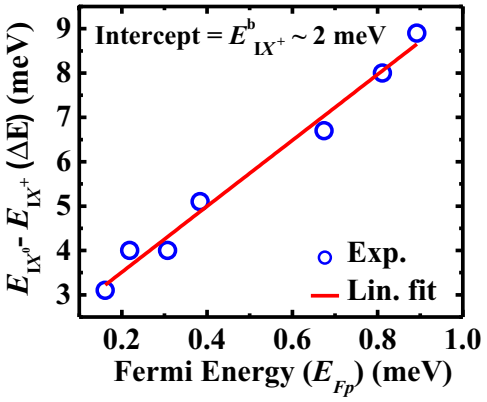

FIG. 3. Variation of peak splitting energy for excitons and trions with respect to the Fermi energy. The estimated trion binding energy matches well with past results in GaAs.

Moreover, we note that dissociation of either excitons or trions inside a solid is always a many-body statistical process with a thermodynamic dissociation probability of approximately $\exp[-(E^b/k_BT)]$, where E^b can be either the exciton or the trion binding energy [23,28,29]. This is because such dissociations are typically governed by the following Saha's ionization equations [28,29]:

$$\frac{n_h n_e}{n_{X^0}} = \frac{C^2_{X^0}}{C^2_e C^2_h}\exp\left(-\frac{E^b_X}{k_BT}\right) \quad \text{and} \tag{12}$$

$$\frac{n_X n_h}{n_{X^+}} = \frac{4C^2_{X^+}}{C^2_X C^2_h}\exp\left(-\frac{E^b_{X^+}}{k_BT}\right), \tag{13}$$

where $E^b_{X^0}$, $E^b_{X^+}$ are the binding energies of excitons and positively charged trions, n_i are carrier densities per unit area, $C_i = \hbar\sqrt{2\pi/m_i k_B T}$ are thermal wavelengths, and m_i are the effective masses of ($i = e$, h, X^0, X^+) electrons, holes, excitons, and trions, respectively, as in Ref. [28].

Most importantly, assuming constant prefactors to the exponential term in Eqs. (12) and (13), we note that $\exp(-2) \approx 0.135$, $\exp(-1) \approx 0.368$, $\exp(-0.5) \approx 0.607$ when the all-important ratio (E^b_i/k_BT) varies from 2 to 1 to 0.5, respectively. This clearly shows that even when the binding energy E^b_i is less than the thermal fluctuation energy (k_BT), there still can be a finite, *nonzero* probability of having some bound states of excitons or trions. It is remarkable to discover that photocapacitance spectroscopy is still sensitive to these very small numbers of excitons or trions. As such, we already know [18] that binding energies can also change under applied bias and can also affect the above populations. However, such changes can be quite small (see Fig. 5(b) of Ref. [18]). Therefore, based on the above numerical estimates, unless the ratio (E^b_i/k_BT) varies greatly, it need not significantly affect the final population.

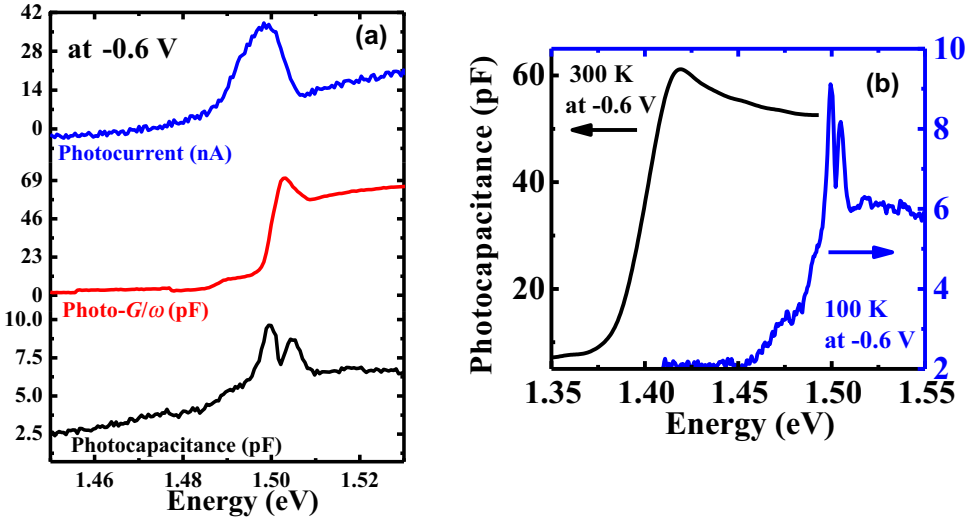

FIG. 4. (a) Photocapacitance and photo-G/ω measured at 200 Hz is compared with dc photocurrent spectra for −0.6 V bias at 100 K. (b) Photocapacitance spectra at 100 and 300 K are compared at a similar reverse bias of −0.6 V and frequency of 200 Hz. Spectral peak energy and spectral shape changed significantly with temperature.

C. Differences in spectra at a fixed bias and with respect to temperature

Photocapacitance and photo-G/ω spectra at 200 Hz are compared with dc photocurrent spectra for a −0.6 V bias at 100 K as shown in Fig. 4(a). Spectral splitting is only observed in photocapacitance spectra whereas we do not see any spectral splitting in photocurrent and photo-G/ω. There is a slight shift in peak energy position observed among these. Such differences are also observed at room temperature and are attributed [18] to dissociation of direct excitons that are not closer to the AlAs potential barrier. We would like to mention here that a simple equivalent circuit consisting of capacitance (C) and conductance (G) in parallel is used to extract photocapacitance using a LCR meter such that $|C|$ is always greater than $|0.1 \times G/\omega|$ where $\omega = 2\pi f$. We know [18] that photocapacitance mainly arises from the bias-driven accumulated charge carriers near the AlAs barrier whereas the dc photocurrent is solely affected by the charge carriers driven out of the junction. However, contributions to photo-G/ω can come from both of these regions. Moreover, one can notice that the spectral broadening in the photocurrent spectra is reasonably higher than the photo-G/ω and photocapacitance at −0.6 V. All of these certainly imply that the origin of dc photocurrent spectra is different. The measured photocurrent is likely to originate from the dissociation of excitonic [30] photoabsorptions, which are mostly forming away from the junction [18]. This will be further elaborated in Sec. III D.

In Fig. 4(b), we now explain how the temperature variation changes the photocapacitance spectral shape and the peak energy for this particular applied bias of −0.6 V. Here, we observe that the single excitonic peak at room temperature drastically changes to narrower double peaks of both excitons and trions at 100 K. This clearly indicates that such peak splitting occurs only at low temperatures and also under high applied biases. Such a critical role of applied biases will again be emphasized in Sec. III D. The blueshift of the spectral peak energies with decreasing temperature can be explained by the usual band gap expansion.

D. Advantages of photocapacitance spectra in comparison to PL spectra in studying such indirect excitonic complexes

In most studies, PL spectra are mainly used to understand the intricate details of many-body carrier dynamics of trions and FES. In Fig. 5(a), we plot the PL spectra

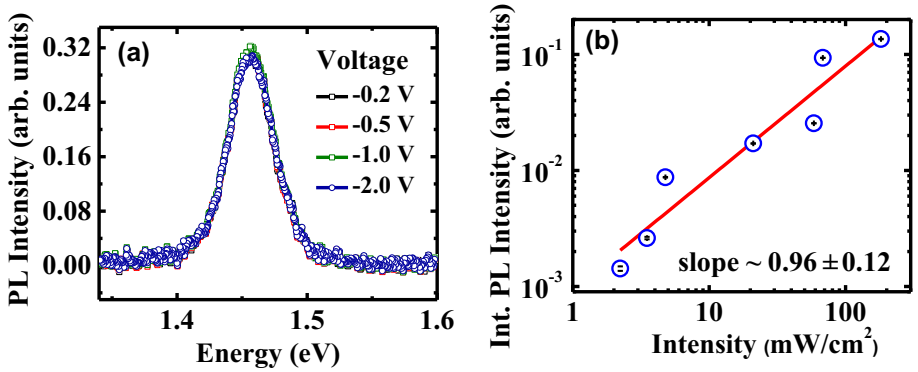

FIG. 5. (a) Photoluminescence spectra at 100 K under different reverse biases. However, we did not observe any bias-dependent spectral splitting and spectral redshift in the photoluminescence spectra. (b) Integrated PL intensity vs excitation intensity follows a linear variation on a log-log plot, which gives a slope of approximately 0.96 at 100 K.

at 100 K for different applied biases. The spectral broadening, i.e., FWHM, is certainly more than that of the usual intrinsic FWHM of any excitonic PL at low temperature. However, unlike photocapacitance spectra, we do not observe spectral splitting and any spectral shift in the PL spectra under increasing reverse biases. This PL spectral peak energy is, as expected, at a lower energy in comparison to the photocapacitance spectral peak. This definitely indicates two different physical origins for PL and photocapacitance spectra. Integrated PL intensity versus optical excitation intensity also follows a linear variation on a log-log scale, which gives a slope of approximately 0.96 at 100 K indicating [26] the presence of excitons as shown in Fig. 5(b). PL spectra are mostly unaffected by the applied bias. PL is also a two-step probabilistic process involving photoexcitation and radiative recombination. It is expected that neutral, indirect excitons (IX^0s) and positively charged, indirect trions (IX^+s) around the AlAs barrier hardly contribute to PL due to the lack of spatial overlap of their respective electron and hole wave functions. Therefore, the observed PL is mainly due to the presence of excitons that are photoexcited far away from the AlAs junction and then radiatively recombine. As a result, PL spectra are hardly affected by the applied bias. However, the indirect excitons, trions (IX^+), and FES forming near the heterojunction are strongly affected by the applied bias as shown in Figs. 1(c) and 1(d). As a result, such bias-induced changes in carrier accumulations around the GaAs/AlAs/GaAs heterojunction can be sensed by photocapacitance.

As such, absorption and emission spectroscopies are based on two different mechanisms where carrier dynamics and detection techniques are different. In fact, this difference is the exact reason why PL is not able to respond to an applied bias and can not probe the all-important indirect excitons at such a high temperature of 100 K even with more intense photoexcitation. This is because electron-hole pairs generated throughout the top GaAs also contribute significantly to PL. On the other hand, the radiative recombinations from spatially indirect excitonic many-body systems are negligible. As reported previously [18] for indirect excitons, the photocapacitance spectroscopy is now shown to also be sensitive to bias-induced dipolar changes of indirect trions and FES formed across the AlAs barrier. It is this enhanced selectivity of photocapacitance spectroscopy to these spatially indirect dipoles of excitonic many-body systems such as trions and FES that needs to be mentioned here. In the present article, we wanted to emphasize that photocapacitance spectroscopy is a superior technique in detecting these delicate indirect excitons, trions, and FES in comparison with conventional PL spectroscopy.

In addition, we want to state that the optical intensity dependence of photocapacitance spectra is also studied for fixed biases at 100 K (spectra are not shown here). Spectral peak splitting and shapes are observed to be hardly affected by the variation of the optical excitation intensity over the range 2–50 μW/cm^2. An increase of the optical excitation intensity only increases the magnitude of the overall photocapacitance. Interestingly, it is the applied bias that plays a more crucial role in injecting the optically generated carriers to respective TQWs to form excitonic complexes. Therefore, we now have experimental proof that formations of these spatially indirect trions and FES in this GaAs/AlAs/GaAs heterostructure can be predominantly controlled by the applied reverse bias and not so much by the optical excitation intensity.

IV. CONCLUSIONS

In summary, photocapacitance spectroscopy is used to detect the formation of spatially indirect, bias-driven dipoles of excitons as well as positively charged trions around the AlAs barrier in a GaAs/AlAs/GaAs *p-i-n* heterostructure even at 100 K. We demonstrate bias-dependent spectral peak splitting of exciton and trions. Moreover, in the higher density limit $\geq 1 \times 10^{11}$ cm^{-2}, we also identify the signatures of FESs from photocapacitance spectra. Contrary to popular belief, the presence of trions at such a high temperature of approximately 100 K in these III-V materials is explained using Saha's ionization equation. This analysis indicates that there is always a small but finite thermodynamic probability of existence of excitonic complexes having binding energy lower than the thermal bath energy (k_BT). Interestingly, we show that these small fractions of trions and excitons do respond to photocapacitance spectroscopy, but not to conventional optical measurements such as PL and dc photocurrent spectra. Researchers usually use PL to study these excitons, trions, and FESs in a variety of materials. However, we establish here that photocapacitance is a superior and sensitive experimental tool to probe and study these types of spatially indirect, many-body excitonic complexes in such single-barrier *p-i-n* heterostructures. Our work also explains why and how photocapacitance spectroscopy can probe these interacting dipoles of trions and FESs, which an ordinary luminescence spectroscopy fails to do.

Such electrical detection and manipulation of excitons and trions at such high temperatures of 100 K is clearly unheard of in III-V materials. We predict that these observations provide a first concrete step toward any device-level experimental control of trions and FESs at even higher temperatures. This can further lead to future applications [3,31–33] in next-generation optoelectronics and telecommunications devices, possibly even at room temperature, using similar heterostructures made with 2D monolayers of TMDC having high excitonic binding energies. Moreover, it is difficult to directly probe the "dark" excitons with standard optical emission-based spectroscopies. However, these kinds of capacitive techniques

[18,26] have the potential to even sense dipolar signatures of "dark" excitons that constitute the true ground state of any excitonic BEC. Such indirect excitons in TMDC heterostructures are also predicted [34,35] to display excitonic superconductivity, electro-optical spectral control of trion lasing [36], and optical modulation [37] of "dipolar" excitons. Therefore, our present and past [18,26] studies on frequency-dependent dynamic signatures of the dipolar nature of excitons and trions can provide significant impetus to explore simple photocapacitive spectral control of excitons, trions, and FESs for future applications.

ACKNOWLEDGMENTS

We acknowledge the Department of Science and Technology, India (Research Grants No. SR/S2/CMP-72/2012 and No. SR/NM/TP13/2016). We are grateful to Professor B. M. Arora from IIT-Mumbai for his advice on band diagrams. A.B. and M.K.S. are grateful to DST, India for the Inspire PhD Program and IISER-Pune for the Integrated PhD Program, respectively. Y.G.G. acknowledges financial support from the Brazilian agency Fundação de Amparo a Pesquisa do Estado de São Paulo (FAPESP) (Research Grants No. 16/10668-7 and No. 18/01808-5). M.H. acknowledges support from the UK Engineering and Physical Sciences Research Council.

[1] B. Ganchev, N. Drummond, I. Aleiner, and V. Fal'ko, Three-Particle Complexes in Two-Dimensional Semiconductors, Phys. Rev. Lett. **114**, 107401 (2015).

[2] M. Zielinski, K. Golasa, M. R. Molas, M. Goryca, T. Kazimierczuk, T. Smolenski, A. Golnik, P. Kossacki, A. A. L. Nicolet, M. Potemski, Z. R. Wasilewski, and A. Babinski, Excitonic complexes in natural InAs/GaAs quantum dots, Phys. Rev. B **91**, 085303 (2015).

[3] L. V. Butov, Excitonic devices, Superlatt. Microstruct. **108**, 2 (2017).

[4] M. A. Lampert, Mobile and Immobile Effective-Mass-Particle Complexes in Nonmetallic Solids, Phys. Rev. Lett. **1**, 450 (1958).

[5] F. M. Peeters, C. Riva, and K. Varga, Trions in quantum wells, Phys. B: Condens. Matter **300**, 139 (2001).

[6] R. A. Sergeev, R. A. Suris, G. V. Astakhov, W. Ossau, and D. R. Yakovlev, Universal estimation of X^- trion binding energy in semiconductor quantum wells, Eur. Phys. J. B **47**, 541 (2005).

[7] F. J. Teran, L. Eaves, L. Mansouri, H. Buhmann, D. K. Maude, M. Potemski, M. Henini, and G. Hill, Trion formation in narrow GaAs quantum well structures, Phys. Rev. B **71**, 161309 (2005).

[8] K. F. Mak, K. He, C. Lee, G. H. Lee, J. Hone, T. F. Heinz, and J. Shan, Tightly bound trions in monolayer MoS2, Nat. Mater. **12**, 207 (2013).

[9] B. Zhu, H. Zeng, J. Dai, Z. Gong, and X. Cui, Anomalously robust valley polarization and valley coherence in bilayer WS2, Proc. Natl. Acad. Sci. U.S.A. **111**, 11606 (2014).

[10] B. Stébé and A. Ainane, Ground state energy and optical absorption of excitonic trions in two dimensional semiconductors, Superlatt. Microstruct. **5**, 545 (1989).

[11] S. Glasberg, G. Finkelstein, H. Shtrikman, and I. Bar-Joseph, Comparative study of the negatively and positively charged excitons in GaAs quantum wells, Phys. Rev. B **59**, R10425 (1999).

[12] G. D. Mahan, Excitons in degenerate semiconductors, Phys. Rev. **153**, 882 (1967).

[13] P. Hawrylak, Optical properties of a two-dimensional electron gas: Evolution of spectra from excitons to Fermi-edge singularities, Phys. Rev. B **44**, 3821 (1991).

[14] G. G. Spink, P. López Ríos, N. D. Drummond, and R. J. Needs, Trion formation in a two-dimensional hole-doped electron gas, Phys. Rev. B **94**, 041410 (2016).

[15] G. Yusa, H. Shtrikman, and I. Bar-Joseph, Onset of exciton absorption in modulation-doped GaAs quantum wells, Phys. Rev. B **62**, 15390 (2000).

[16] W. Chen, M. Fritze, A. V. Nurmikko, M. Hong, and L. L. Chang, Fermi-edge singularities and enhanced magnetoexcitons in the optical spectra of GaAs/(Ga,Al)As single quantum wells, Phys. Rev. B **43**, 14738 (1991).

[17] M. S. Skolnick, J. M. Rorison, K. J. Nash, D. J. Mowbray, P. R. Tapster, S. J. Bass, and A. D. Pitt, Observation of a Many-Body Edge Singularity in Quantum-Well Luminescence Spectra, Phys. Rev. Lett. **58**, 2130 (1987).

[18] A. Bhunia, M. K. Singh, Y. G. Gobato, M. Henini, and S. Datta, Experimental evidences of quantum confined 2D indirect excitons in single barrier GaAs/AlAs/GaAs heterostructure using photocapacitance at room temperature, J. Appl. Phys. **123**, 044305 (2018).

[19] H. V. A. Galeti, H. B. de Carvalho, M. J. S. P. Brasil, Y. Galvão Gobato, V. Lopez-Richard, G. E. Marques, M. Henini, and G. Hill, Role of X valley on the dynamics of electron transport through a GaAs/AlAs double-barrier structure, Phys. Rev. B **78**, 165309 (2008).

[20] J. J. Finley, R. J. Teissier, M. S. Skolnick, J. W. Cockburn, G. A. Roberts, R. Grey, G. Hill, M. A. Pate, and R. Planel, Role of the X minimum in transport through AlAs single-barrier structures, Phys. Rev. B **58**, 10619 (1998).

[21] J. Singh, *Physics of Semiconductors and Their Heterostructures* (McGraw-Hill Inc., USA, New York, 1992).

[22] E. E. Vdovin, M. Ashdown, A. Patanè, L. Eaves, R. P. Campion, Y. N. Khanin, M. Henini, and O. Makarovsky, Quantum oscillations in the photocurrent of GaAs/AlAs p-i-n diodes, Phys. Rev. B **89**, 205305 (2014).

[23] A. Vercik, Y. G. Gobato, and M. J. S. P. Brasil, Thermal equilibrium governing the formation of negatively charged excitons in resonant tunneling diodes, J. Appl. Phys. **92**, 1888 (2002).

[24] H. Kalt, K. Leo, R. Cingolani, and K. Ploog, Fermi-edge singularity in heavily doped GaAs multiple quantum wells, Phys. Rev. B **40**, 12017 (1989).

[25] A. Bugajski and K. Reginski, Optical properties of semiconductor quantum wells, Opto-Electron. Rev. **4**, 97 (1996).

[26] A. Bhunia, K. Bansal, M. Henini, M. S. Alshammari, and S. Datta, Negative activation energy and dielectric signatures of excitons and excitonic Mott transitions in quantum confined laser structures, J. Appl. Phys. **120**, 144304 (2016).

[27] V. Huard, R. T. Cox, K. Saminadayar, A. Arnoult, and S. Tatarenko, Bound States in Optical Absorption of Semiconductor Quantum Wells Containing a Two-Dimensional Electron Gas, Phys. Rev. Lett. **84**, 187 (2000).

[28] A. Esser, E. Runge, R. Zimmermann, and W. Langbein, Trions in GaAs quantum wells: Photoluminescence lineshape analysis, Phys. Status Solidi A **178**, 489 (2000).

[29] J. Szczytko, L. Kappei, J. Berney, F. Morier-Genoud, M. T. Portella-Oberli, and B. Deveaud, Determination of the Exciton Formation in Quantum Wells from Time-Resolved Interband Luminescence, Phys. Rev. Lett. **93**, 137401 (2004).

[30] M. Fox, *Optical Properties of Solid*, 2nd edn. (Oxford University Press Inc., USA, New York, 2010).

[31] V. Orsi Gordo, M. A. G. Balanta, Y. Galvão Gobato, F. S. Covre, H. V. A. Galeti, F. Iikawa, O. D. D. Couto, Jr., F. Qu, M. Henini, D. W. Hewak, and C. C. Huang, Revealing the nature of low-temperature photoluminescence peaks by laser treatment in van der Waals epitaxially grown WS2 monolayers, Nanoscale **10**, 4807 (2018).

[32] W. Xia, L. Dai, P. Yu, X. Tong, W. Song, G. Zhang, and Z. Wang, Recent progress in van der waals heterojunctions, Nanoscale **9**, 4324 (2017).

[33] A. Pospischil and T. Mueller, Optoelectronic devices based on atomically thin transition metal dichalcogenides, Appl. Sci. **6**, 78 (2016).

[34] M. M. Fogler, L. V. Butov, and K. S. Novoselov, High-temperature superfluidity with indirect excitons in van der Waals heterostructures, Nat. Commun. **5**, 4555 (2014).

[35] O. L. Berman and R. Y. Kezerashvili, High-temperature superfluidity of the two-component Bose gas in a transition metal dichalcogenide bilayer, Phys. Rev. B **93**, 245410 (2016).

[36] J. Puls, G. V. Mikhailov, F. Henneberger, D. R. Yakovlev, A. Waag, and W. Faschinger, Laser Action of Trions in a Semiconductor Quantum Well, Phys. Rev. Lett. **89**, 287402 (2002).

[37] S. Yu, X. Wu, Y. Wang, X. Guo, and L. Tong, 2D materials for optical modulation: challenges and opportunities, Adv. Mater. **29**, 1606128 (2017).

Correction: Minor errors in text have been fixed.